Research article

Dynamic expansion of mesenchymal stem/stromal cells in a stirred tank bioreactor promotes the release of potent extracellular vesicles

Jan Barekzai[1], Jonas Friedrich[1], Maduwuike Okpara[1], Laura Refflinghaus[1], Dustin Eckhardt[1], Peter Czermak[1,2] and Denise Salzig[1,2,*]

[1] Institute of Bioprocess Engineering and Pharmaceutical Technology, University of Applied Sciences Mittelhessen, 35390 Giessen, Germany

[2] Faculty of Biology and Chemistry, Justus-Liebig-University of Giessen, 35390 Giessen, Germany

* Correspondence: Email: denise.salzig@lse.thm.de; Tel: +496413092630; Fax: +496413092553.

Abstract: Mesenchymal stem/stromal cell-derived extracellular vesicles (MSC-EVs) are considered a promising therapeutic tool in cell therapy due to their immunomodulatory, regenerative and angiogenic capabilities. However, there is a lack of process knowledge, particularly for a large-scale production of MSC-EV using fully controlled stirred tank bioreactor (STR) systems. For the establishment of a STR-based process, we investigated dynamic process set-ups in spinner flasks, using three different microcarriers, as well as in shaking flasks, using microcarrier-free spheroids. An immortalized cell line (hMSC-TERT) and a particle-free chemically defined medium was used for all approaches. Cell characteristics (e.g., growth, metabolism, cell-specific particle production rates), MSC-EV epitope markers and MSC-EV potency in migration assays were analyzed. We showed that the transfer to a dynamic system (non-porous microcarrier, spinner flask) significantly increased the cell-specific particle production rate (6-fold) and the expression of EV-specific markers. Moreover, MSC proliferation and, most importantly, the therapeutic potency of MSC-derived particles including EVs was maintained. We demonstrated that high cell-specific particle production rates were associated with an increased glucose consumption rate rather than cell growth, which can be utilized for future process development. Furthermore, we showed that dynamic conditions of a controlled 1 L STR significantly increased the cell-specific particle production rate (24-fold) as well as the final concentration (3-fold) of potent MSC-derived particles including EVs. This indicates that fully controlled STRs are an efficient production system for MSC-derived particles including EVs that may open and facilitate the path for clinical applications.

1.   Introduction

Mesenchymal stem/stromal cells (MSCs) represent a powerful tool for therapeutic approaches in medicine, especially for cell therapy and tissue engineering. Numerous clinical trials have already demonstrated the potential of MSCs for the treatment of non-curable diseases such as the graft-versus-host disease (GvHD), myocardial injuries, diabetes, ischemic stroke or liver diseases [1]. This is due to their multipotent, immunomodulatory, anti-inflammatory and regenerative properties [2]. For regenerative medicine, the properties related to tissue repair are of particular interest [3]. These include effects such as the migration to sites of injury, angiogenesis and anti-scarring effects. MSCs were originally thought to exert their therapeutic effect by migrating to the therapeutic site and subsequently differentiating into the desired cell type. However, therapeutic effects of MSCs can be observed a long time after transplantation, although several studies have revealed a low MSC engraftment rate after transplantation [4]. This increasingly suggests that therapeutic effects are not only caused by direct cell-cell contacts or the replacement of defective cells by newly differentiated MSCs, but rather by paracrine effects of MSCs. In addition to soluble growth factors and cytokines, extracellular vesicles (EVs) are of increasing importance for therapeutical applications [4]. As an important component of cell-cell communication, EVs are involved in cellular and pathophysiological processes such as angiogenesis, immune response, homeostasis maintenance, cancer progression, proliferation and differentiation. EVs perform their therapeutic functions by acting as intercellular shuttles, transferring biologically active molecules such as proteins, DNA, RNA (mRNA and miRNA) and lipids between cells [5]. Indeed, recent studies have already shown beneficial effects of MSC-EVs in various disease models, such as the GvHD, stroke, sepsis, kidney injury or skin wound healing [5].

For the clinical translation of MSC-EVs, a suitable, scalable and GMP-compliant production platform is required, since cell and EV properties are affected by biological, chemical, physical and mechanical process parameters [6]. Different static and dynamic, as well as 2D and 3D, systems for the EV production of anchorage dependent MSCs are already investigated on a laboratory scale. Often, MSC-EVs are produced under static conditions, using 2D plastic surfaces, such as T-flasks. Disadvantages of a static 2D culture are the formation of substrate and pH gradients, a lack of process scalability and a lack of suitable online monitoring techniques necessary to meet GMP requirements. Furthermore, 2D cultures poorly mimic the physiological environmental conditions of MSCs *in vivo*, which could decrease the quantity and quality of secreted EVs compared to 3D cultures [7,8]. The solution could be bioreactors that offer a dynamic environment with many options for process control and optimization, where process parameters such as temperature, pH, dissolved oxygen and biomass can be monitored and adjusted easily. Furthermore, a homogeneous microenvironment prevents the formation of substrate gradients or accumulation of toxic products, which can inhibit cell growth and EV productivity.

Different bioreactor systems have been investigated for MSC-EV production. Cao et al. reported a 19.4-fold increase in a total exosome production in a hollow fiber bioreactor in which MSCs form high density cell clusters [9]. In the vertical-wheel reactor, a 5.7-fold increase of the EV concentration and a 3-fold increase in productivity in a serum/xeno-free microcarrier-based culture, compared to

static conditions, was reported [8]. A stirred-tank bioreactor (STR) offers a variety of process set-ups for the dynamic culture of MSCs and the production of MSC-EVs. MSCs can be grown as spheroids, or a growth surface can be provided as spheres with 100-300 μm in diameter, known as microcarriers. Cha *et al.* showed a 100-fold increased EV production in a dynamic 3D spheroid culture of MSCs using a microwell approach [10]. A microcarrier-based spinner flask culture also increased the exosome yield in the conditioned medium of umbilical cord MSCs [11]. Most recently, a study described a controlled microcarrier-based STR process in a fed-batch and perfusion mode that maximized MSC proliferation and isolated EV from conditioned medium with no significant differences in EV size and concentration [12]. However, there is no description of the effect of the hydrodynamic conditions or microcarrier properties on the EV production in dynamic culture conditions, especially in comparison to classical static production systems. In addition, the absence of correlations between cell- and EV-specific properties represents a significant challenge. This limitation is particularly challenging when EVs with specific attributes, such as size, surface markers or potency, are desired. The attainment of a rationally designed EV-product for personalized medicine can only be realized by acquiring more process knowledge in well characterized, scalable EV production systems [13]. Although some first studies showed the beneficial effect of a dynamic MSC-EV production, fundamental process knowledge is currently lacking. Almeria et al. reviewed the impact of the culture conditions on MSC-EV production [6]. The authors concluded that 3D and dynamic MSC-EV production processes are superior to traditional 2D culture in terms of yield and angiogenic, anti-inflammatory and immunomodulatory properties of MSC-EVs. However, they underscored the importance of further process development in this area, as the influence of relevant process parameters on the production of MSC-EVs have been poorly investigated so far.

In addition, the cultivation medium affects MSCs and is therefore important for successful and efficient EV production. Serum is often added to the cultivation medium [3]. However, Kornilov et al. showed a high contaminating particle load of 2.5×10^{11} particles mL^{-1} in serum, which complicates the production, isolation and analysis of MSC-EVs [14,15]. Bovine-EVs can be removed elaborately by ultracentrifugation. However, this method is time-consuming and lacks scalability [15]. To circumvent the removal of exogenous EVs prior to usage, the so-called starving method is often used. For this, MSCs are cultured and expanded in a serum-containing medium. For the EV-production phase, the serum-containing medium is replaced with serum-free or chemically defined medium for EV production [16]. However, this method provides several disadvantages such as additional operation steps during cell culture, increasing the probability of contamination. Similarly, undefined serum residues may be present, reducing process stability and reproducibility. Most importantly, the method of starvation is limited in time, as excessive starvation time can cause MSCs to enter an apoptotic state, which ultimately affects EV properties. These issues give rise to the urgency for a GMP-compliant process in which MSC-EVs are produced in MSC-expansion processes in chemically defined conditions and on a large scale.

Several studies investigated the expansion of MSCs in dynamic conditions [17–20] focusing exclusively on MSC growth and properties. As only little knowledge on the investigation of an MSC-EV production process has been published so far, we focused mainly on the production of particles including EVs and on possible correlations with specific cell-based process parameters. As we used a chemically defined medium with a non-detectable particle background, we needed a minimal processing of supernatants to analyze the MSC-derived particles including EVs. We were aware that other particles besides EVs might be present in the supernatants. However, we examined the

therapeutic potency if the supernatants i) showed an expression of EV- and MSC-specific markers (CD81, CD63, CD9 and CD44, CD29, respectively), confirming the presence of MSC-EVs [21] and ii) contained particles within the MSC-EV typical size range. We investigated three different types of microcarriers, consisting of different materials and different porosities, in spinner flasks and compared them to a standard cell culture in T-flasks. Here, higher porosities were assumed to favor the migration of MSCs into the microcarrier interior, where minimal shear effects from the stirrer or microcarrier collisions should prevail, while providing the same nutrient supply as on the microcarrier surface. In addition, a microcarrier-free production was investigated in the form of a spheroid culture to mimic physiological *in vivo* conditions of a cell compartment. We compared cell- and EV-specific characteristics, including growth, metabolism, cell-specific EV production rates, EV epitope markers and potency in migration assays with HaCaT cells. Based on the screening experiment, in which the most suitable production platform was identified, a process transfer to a monitored and controlled 1 L stirred bioreactor was performed.

2.   Materials and methods

2.1. Cell culture

2.1.1.   Routine cell expansion

hMSC-TERT (kindly provided by Prof. M. Kassem [22]) were cultured in CellBIND tissue culture flasks (Corning, New York, USA) containing the chemically defined SteMaxOne (Cell Culture Technologies, Gravesano, Switzerland) and 0.2% (v/v) of an Insulin-Transferrin-Selenium mixture (100×, Gibco, Schwerte, Germany) which will further be referred to as MSC growth medium with a seeding density of 4,000 cells cm^{-2}, cultured at 37 °C and 8% CO_2 in a humidified atmosphere. Before passaging, the cells were observed by microscopy to ensure the absence of morphological defects and contamination. Passaging was performed at 80–90% confluence using 0.026 mL·cm^{-2} TrypLE (Gibco, Schwerte, Germany) for 1 min at room temperature.

HaCaT cells, a spontaneously immortalized human keratinocyte line (Cell Lines Services, Germany), were cultured in high glucose DMEM (Gibco, Schwerte, Germany) containing L-glutamine supplemented with 10% (v/v) fetal calf serum (Sigma-Aldrich, Taufkirchen, Germany) at 37 °C and 5% CO_2 in a humidified atmosphere. Cells were seeded at 4,000 cells cm^{-2}. Before passaging, the cells were observed by microscopy to ensure the absence of morphological defects and contamination. When 80–90% confluence was reached, the cells were washed using phosphate buffered saline (PBS, Biochrom) and detached using 0.026 mL·cm^{-2} TrypLE for 10 min.

2.1.2.   Static growth

For capturing static growth- and particle-production kinetics, hMSC-TERT were cultured in 6-well plates (Corning, New York, USA) containing MSC growth medium with a seeding density of 4,000 cells cm^{-2} for ten days (37 °C, 8% CO_2, humidified atmosphere). The supernatant was sampled daily, centrifuged at 1,000 × g for 10 min and stored at −80 °C for later analysis. The cells were detached using TrypLE, followed by daily cell count using a Neubauer hemocytometer. For a migration assay, three T75 flasks were cultured for 168 h at similar conditions as in 6-well plates

(MSC growth medium, 37 °C, 8% CO_2 in a humidified atmosphere) to produce supernatants, which were then centrifuged at 1,000 × g for 10 min and stored at −80 °C.

2.1.3. Microcarrier screening in spinner flasks

For expansion and MSC-derived particle production including EVs of hMSC-TERT, three microcarrier types with different porosities were investigated as triplicates in spinner flasks (magnetic pendulum, Integra Biosciences, Wallisellen, Switzerland) with a 100 ml working volume. Cytodex 1 and Cytopore 2 microcarriers (Cytiva, formerly GE Healthcare, Solingen, Germany) were prepared as recommended by manufacturer instructions before sterilization. Enhanced attachment microcarriers (Corning, New York, USA) were sterile and ready to use. Table 1 summarizes the microcarrier specifications. After 1 h equilibration of MSC growth medium at 37 °C and 8% CO_2 in a humidified atmosphere, all spinner flasks were inoculated at 4,000 cells cm^{-2}. The initial stirrer speed was set to 20 rpm to facilitate cell attachment. The stirring speed was increased to a maximum of 40 rpm during culturing to avoid microcarrier agglomeration. 2 mL of the microcarrier-cell suspension were sampled daily, where the supernatant was centrifuged at 1,000 × g for 10 min and stored at −80 °C until analysis. The cells were detached from the microcarriers using TrypLE for 5 min and gentle pipetting. The detachment was confirmed by microscopical observation. The cell count was done by using a Neubauer hemocytometer. After 168 h, the total supernatant was centrifuged at 1,000 × g for 10 min and stored at −80 °C for the migration assay analysis.

Table 1. Microcarrier properties used in spinner and STR experiments.

Microcarrier	Manufacturer	Porosity and material	Concentration in culture [$g \cdot L^{-1}$]	Specific surface [$cm^2 \cdot g^{-1}$]	Diameter [μm]
Enhanced Attachment (EA)	Corning	Non-porous, polystyrene	15	360	125–212
Cytodex 1 (CD)	Cytiva, formerly GE Healthcare	Micro-porous, dextran beads	3	4400	190
Cytopore 2 (CP)	Cytiva, formerly GE Healthcare	Macro-porous, cross-linked cotton cellulose	3	11000	230

2.1.4. Spheroid formation in shaking flasks

Spheroid formation was recently published [23] and is therefore only described shortly. Dynamic spheroid formation was carried out in MSC growth medium in shaking flasks at 37 °C in a 5% CO_2 in a humidified atmosphere for five days. We used a 100 mL baffled shaking flask with a working volume of 20 mL on a shaking plate (Infors HT, Bottmingen, Switzerland) at 100 rpm with an eccentricity of 2.5 cm. All flasks were inoculated at a seeding density of 2.5 × 10^5 cells mL^{-1}. Daily samples were stained with calcein/ethidium to test vitality, and an image-based analysis of the spheroid

size distribution was carried out according to Petry *et al.* [23] and supernatants frozen at −80 °C for later analysis. After 120 h, the total supernatant was centrifuged at 1,000 × g for 10 min and stored at −80 °C for migration assay analysis.

2.1.5. Process transfer into a fully controlled stirred tank bioreactor

For a large-scale production of MSC-derived particles including EVs, we used the Labfors 5 bioreactor system (Infors HT, Bottmingen, Switzerland). The inner tank diameter was 0.115 m with a dished bottom. The working volume was 1 L, resulting in a ratio of liquid height to tank diameter of 1. We used a 45 three-segmented pitched-blade stirrer at a stirring speed of 57 rpm, ensuring a complete suspension of all microcarriers, according to Zwietering et al. [24]. The STR was equipped with process analytical technology, including a pH probe, a temperature probe, a dissolved oxygen probe and a dielectric spectroscopy probe (all from Hamilton, Bonaduz, Switzerland). The pH was set to 7.3 ± 0.1 and down-regulated by adding CO_2 over headspace and up-regulated by adding 1 M sodium hydroxide. The temperature was kept constant at 37 °C. The dissolved oxygen (DO) value was kept over 40% by discontinuous aeration over headspace. The four installed probes, the shaft guide, the sparger and pipes for sampling and harvesting were used as baffles and lead to a completely baffled system [25]. After sterilization, the STR was filled with 0.9 L MSC growth medium containing 15 g·L^{-1} enhanced attachment microcarriers and was then equilibrated for 1 h at 37 °C, pH 7.3 ± 0.1 and at a stirring speed of 57 rpm to allow pH and temperature to adjust. A continuous headspace aeration at 50 mL·min^{-1} with air (oxygen partial pressure of 21%) was also applied to allow a DO calibration of 100%. hMSC-TERT were detached from two T175 flasks (MSC growth medium, 37 °C, 8% CO_2 in a humidified atmosphere) and resuspended in 100 mL pre-equilibrated MSC growth medium for an inoculation density of 4,000 cell cm^{-2}. Daily sampling was done as described in section 2.1.3. At the end of culture (STR 1: 192 h, STR 2: 144 h, STR 3: 168 h), the total supernatant was centrifuged at 1,000 × g for 10 min and stored at −80 °C for the migration assay analysis.

2.1.6. Sample preparation

All supernatants were centrifuged at 1,000 × g for 10 min and stored at −80 °C for later analysis. For the migration assay, a suitable control for each sample was needed. 15 mL of each sample were purified using an Amicon ultra 100 kDa centrifugal filter device (Darmstadt, Merck; 1,000 × g for 5 min) to generate a respective control without particles in the permeate (EV-depleted fraction), but with the same metabolic concentrations as in the untreated supernatant.

2.2. Analytical methods and calculations

2.2.1. Determination of growth rate and expansion factor

The growth rate μ was determined during the exponential growth phase using the following equation:

$$\text{Growth rate } \mu \text{ [h}^{-1}\text{]} = \frac{\ln(x_i) - \ln(x_{i-1})}{t_i - t_{i-1}}, \tag{1}$$

where x represents the cell count at the corresponding time point t. The expansion factor represents the ratio of the maximum cell count to the starting cell count:

$$\text{Expansion factor} = \frac{x_{max}}{x_{start}} \tag{2}$$

2.2.2. MSC surface marker analysis

The Stemflow™ human MSC analysis kit from (BD Biosciences, Heidelberg, Germany) includes four positive markers labeled with different fluorochromes (CD90-FITC, CD105-PerCPCy5.5, CD73-APC, CD44-PE) and five negative markers (CD45, CD34, CD11b, CD19, HLA-DR), all of which are labeled with PE. The kit also comes with corresponding isotype controls. To conduct the analysis, microcarriers were rinsed with PBS and hMSC-TERT were detached using TrypLE. hMSC-TERT were immediately stained according to the protocol provided by BD Biosciences. The analysis was performed on a flow cytometer (Guava easycyte 6HT-2L, Darmstadt, Merck).

2.2.3. Spheroid characterization

Data of our spheroid characterization was recently published by our group [23]. Here, we used the same protocol for the assessment of spheroid vitality and spheroid size.

2.2.4. Glucose/Lactate measurement

Glucose and lactate concentrations were determined daily, using a Biosen C-line analyzer (EKF Diagnostic, Barleben, Germany). The following equation was used for the calculation of cell specific conversion rates:

$$\text{Metabolic conversion rate } [\text{g cell}^{-1}\ \text{h}^{-1}] = \frac{(c_i - c_{i-1}) * V}{\bar{x} * (t_i - t_{i-1})} \tag{3}$$

with

$$\text{Logarithmical average cell count } \bar{x} = \frac{x_i - x_{i-1}}{\ln(x_i) - \ln(x_{i-1})}\ , \tag{4}$$

where c represents the metabolite concentration and V represents the working volume at the corresponding time point t.

2.2.5. Particle quantification

For a particle size and concentration determination, a nanoparticle tracking analysis (NTA) was performed with a Nanosight LM10 instrument (Malvern Panalytic, Kassel, Germany) equipped with the NTA 3.0 analytical software, detecting particles from 100–1,000 nm in size. All samples were diluted with pure medium for a final concentration of 10^8–10^9 particles mL^{-1} and measured for 30 s. The video was captured at a camera level of 16, a camera gain of 1, a temperature of 25 °C, a viscosity of 0.9 mPa s and analyzed at an automated detection threshold and blur. For particle sizes, the mean

values and their standard deviations of at least three independent experiments are shown. The particle production rate per cell and time is only valid for the exponential growth phase of each experiment and was calculated using the following equation:

$$\text{Particle production rate [particles cell}^{-1}\text{ h}^{-1}] = Y_{p/x} * \mu, \tag{5}$$

where $Y_{p/x}$ represents the particle yield of produced particles per cell. The particle yield was determined by the linear regression of the total particle count over the cell count and is represented by its slope. For the particle production rate in spheroid cultivations, we used Eq 3, where c_i represents the particle concentration at corresponding time points. The mean particle sizes reflect the mean particle sizes over the entire course of cultivation and not just that of a specific point in time.

2.2.6. Surface marker characterization of EVs by MACSPlex Exosome Kit

For sample preparation, the manufacturer's protocol "Overnight protocol for the assay using 1.5 mL tubes" (Miltenyi Biotec, Germany) was followed. Briefly, pre-cleared cell culture supernatant (centrifugation at $1,000 \times g$, 10 min) containing 3.7×10^8 particles and equal volumes of the blank (medium) were diluted with MACSPlex buffer to a final volume of 120 µL and then mixed with 15 µL of MACSPlex exosome capture beads in 1.5 mL tubes. The mixture was incubated overnight at room temperature and in the absence of light, using an orbital shaker (450 rpm). After washing the beads with 500 µL MACSPlex buffer, 15 µL of MACSPlex exosome detection reagent containing APC-conjugated antibodies (anti-CD9, anti-CD63 and anti-CD81), were added to the mixture. This was followed by a 1 h incubation using an orbital shaker (450 rpm). Beads were washed twice with 500 µL MACSPlex buffer prior to the analysis in the flow cytometer (Guava easycyte 6HT-2L, Darmstadt, Merck). The marker expression of EV-specific markers CD81, CD63, CD9 and MSC-specific markers CD44, CD29, is displayed as the background corrected mean fluorescence intensity (MFI).

2.2.7. Potency in a migration/scratch assay

Potency was assessed in a migration/scratch assay using HaCaT cells. For this, the HaCaT cells were seeded at 7×10^4 cells cm^{-2} in 6 well plates (Sarstedt, Nümbrecht, Germany). After 48 h, two scratches with a length of 1.5 cm were made per well in the cell monolayer using a 1,000 µL pipette tip. Care was taken to ensure that the surface of the well was not damaged. The medium was aspirated and the cells were washed twice with PBS. Each sample was diluted with its corresponding control (see 3.1.6) to a total particle concentration of 2×10^9 particles mL^{-1}. 2 mL of the sample or the corresponding control were transferred into the well. The initial conditions of both 1.5 cm scratches were recorded by microscopy at 200× magnification. After 22 h, both scratches were recorded again by microscopy. By subtraction of the cell confluence at 22 h and 0 h, the total migration of the sample and its control was calculated. The particle-mediated migration was then calculated as the difference of the total migration of the sample and its control in %. Each sample was measured as biological triplicate and technical triplicate (one technical replicate equals two 1.5 cm scratches). For the confluence image analysis, the open-source software Phantast by Jaccard [26] was used.

2.2.8. Statistical analysis

If not stated otherwise, all experiments were performed as three independent runs and presented as mean value ± standard deviations (SD). For a statistical analysis, the following tests were applied: (1) two groups: Student's t-test, (2) for more than two groups: one or two-way ANOVA followed by a post-hoc analysis, using Tukey's test. Intervals of significance were indicated as follows: $* p < 0.05$, $** p < 0.01$, and $*** p < 0.001$.

3. Results and discussion

3.1. Small-scale screening of a suitable MSC expansion platform for an EV production

3.1.1. MSC growth under dynamic conditions

Currently, limited process knowledge is available for the production of MSC-derived particles including EVs, wherefore this work investigated both cell-related and particle/EV-related properties in the manufacturing of MSCs-EVs. The basis for an efficient large-scale MSC-EV production is the use of a scalable culture system, in which cells proliferate to produce sufficient cell numbers starting from a small inoculum. Therefore, a bioreactor system using microcarriers or a spheroid culture are viable options. In our study, MSCs grew in dynamic conditions on non-porous enhanced attachment (EA) and micro-porous Cytodex 1 (CD) microcarriers, but not on macro-porous Cytopore 2 (CP) microcarriers or as spheroids (Figure 1A and Table 2). We determined a decreased cell growth with increasing microcarrier porosity. In comparison of non-porous EA and micro-porous CD microcarriers, MSCs on CD microcarriers had a 45% lower growth rate and a 15.5-fold lowered expansion factor. Although macro-porous CP microcarriers provide a large surface area, MSCs were more likely captured in the periphery of CP microcarriers without cellular spreading or any cell migration inside the microcarrier. Similar observations were published by Yang et al., who determined that MSCs did not grow on CP microcarriers [27]. Compared to the static control (ST), MSCs on non-porous EA microcarriers had a 16.5% higher growth rate, but no significant differences in the expansion factor. The growth rate and the expansion factor of MSCs on micro-porous CD microcarriers were 35.5% and 11.8-fold lower, respectively, compared to ST. Our observations were consistent with Yang et al., who observed a reduced MSC growth on micro-porous CD microcarriers compared to non-porous microcarriers [27] and previously published MSC growth rates [17,28,29]. Thus, based on MSC growth, non-porous EA microcarriers provided the most suitable growth surface while MSC-specific surface markers were not affected (Supplementary Figure 1).

Microcarrier-free dynamic conditions led to MSC aggregation and finally to spheroid formation. Thereby, spheroids showed a constant sauter diameter d_s over time of 46.7–49.5 µm with a high vitality of 96%. As already described by Petry et al. [30], no cell/spheroid growth was observed and, consequently, no growth rate was determined. Petry et al. explained the absence of spheroid growth mainly by surface-erosive effects of prevailing hydrodynamic forces [30].
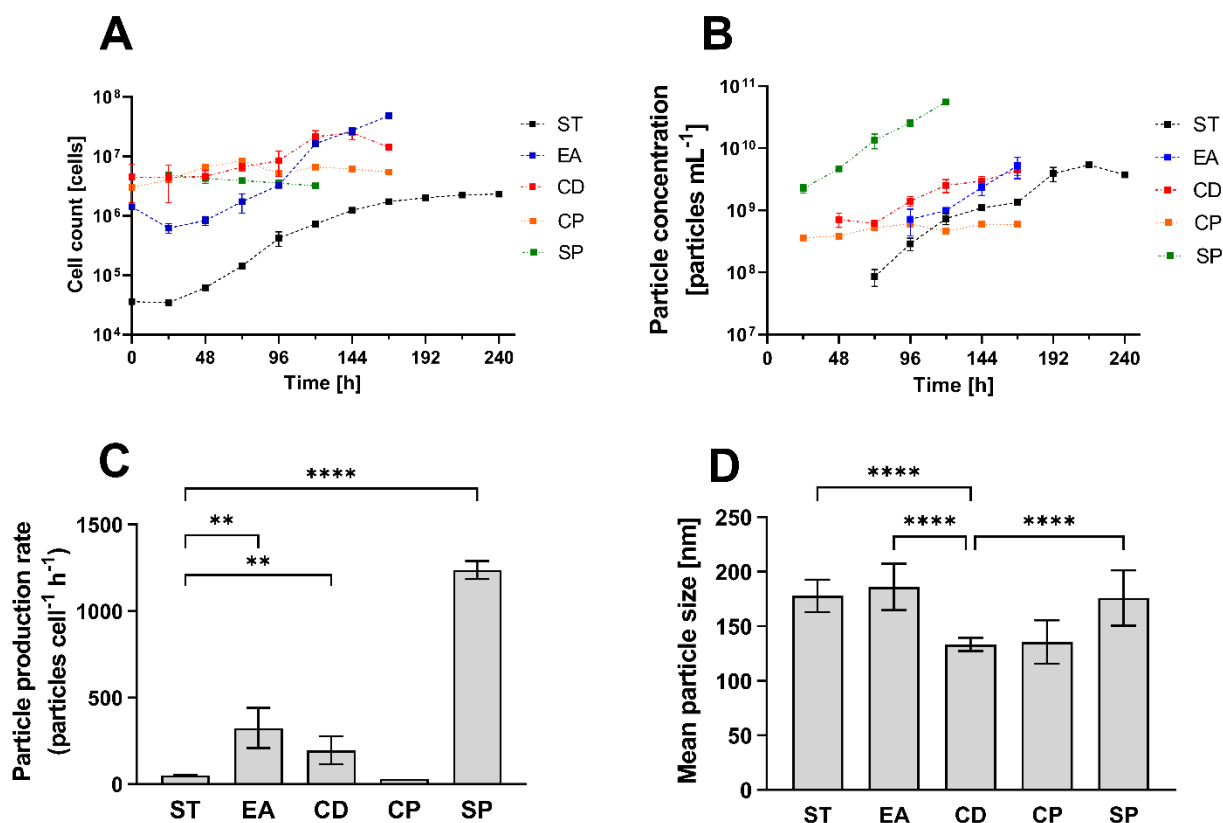
Figure 1. Analysis of MSC growth and particle production in a static system (ST), on different microcarriers in spinner flasks (Enhanced Attachment (EA), Cytodex 1 (CD), Cytopore 2 (CP)) or as spheroids (SP). (A) MSC growth given by total cell count. (B) Particle concentration over time. (C) Particle production rate over the exponential growth phase (ST: 24–144 h, EA: 48–168 h, CD: 48–120 h). (D) Mean particle sizes in supernatants. Data are presented as means $\pm$ SD (n = 3).

3.1.2. Particle production

We analyzed the particle production directly from the cell-free supernatants of the culture. The particles in the supernatant were solely attributed to MSC-derived particles, since the chemically defined medium we used for all experiments were almost particle-free (particle load below detection limit of NTA, $<10^8$ particles mL^{-1}), even after a cultivation for 72 h, using only microcarriers (without cells) to examine the microcarrier-derived particles. For MSCs expanded on EA, CD, and ST, the particle concentration in the supernatant increased exponentially in alliance with the exponential cell growth (Figure 1A, B). The assumption that the particle formation is growth-associated was confirmed by an almost constant particle concentration using CP microcarriers, where MSC did not grow. However, the MSC spheroids, which did not grow, also showed an exponential increase in particles. The particle concentrations (ranging from 4.4–5.4 $\times$ 10^9 particles mL^{-1}) in the ST control and the dynamic EA and CD cultures were in accordance with literature data from hMSC-TERT-derived EVs ranging from 2.5 $\times$ 10^9 particles mL^{-1} [31] to 6.4 $\times$ 10^{11} particles mL^{-1} [32]. No differences in particle concentrations were observed between ST, EA and CD cultures. However, lower final cell

concentrations in EA cultures compared to the ST control indicated increased particle production per cell in dynamic cultures. The comparison of particle concentrations with results of other groups lack in important considerations such as working volume, cell count and time of production. We therefore used the particle production rate as a suitable basis for the comparability of the individual production platforms. The particle production rates (Figure 1C) were 6.6-fold and 4.0-fold higher for EA and CD and 44.2-fold higher for SP, compared to the ST control. Although there might be an impact of growth on the particle formation, we found no general correlation between the MSC growth rate and the particle production rate, e.g., the ST control showed a high growth rate, but only a low particle formation rate (Figure 1C, Table 2).

Interestingly, dynamic conditions increased particle production rates and metabolite conversion rates in a similar manner. Here, the glucose consumption rates (Table 2) were 3.7-fold (EA) and 2.3-fold (CD) higher in dynamic microcarrier cultures than in ST. We determined a linear correlation ($R^2 = 0.998$) between particle production rates and glucose consumption rates. Compared to the ST control, the lactate formation rates were 1.8-fold (EA) and 1.9-fold (CD) increased in dynamic microcarrier cultures. A similar observation was made by Wang et al., who attributed an improved exosome secretion to an improved metabolic activity, rather than to an increased cell number [33].

Table 2. Overview of relevant biological properties of MSCs and produced particles in a static system (ST), on different microcarriers in spinner flasks (Enhanced Attachment (EA), Cytodex 1 (CD), Cytopore 2 (CP)) or as spheroids (SP). Data are presented as means ± SD (n = 3).

System	Growth rate [h^{-1}]	Expansion factor [-]	Particle yield [10^3 Particles cell^{-1}]	Glucose consumption rate [10^{-12} g·cell^{-1}h^{-1}]	Lactate production rate [10^{-12} g·cell^{-1}h^{-1}]
ST	0.0310 ± 0.0007	67.4 ± 8.5	1.6 ± 0.1	70 ± 5	81 ± 5
EA	0.0361 ± 0.0015	88.6 ± 21.7	9.0 ± 2.6	261 ± 25	145 ± 13
CD	0.020 ± 0.004	5.7 ± 4.0	9.7 ± 3.3	163 ± 23	150 ± 21
CP*	-	-	-	114	109
SP	-	-	-	46 ± 8	38 ± 6

Another parameter for a process evaluation of different production platforms is the total particle yield. Strikingly, dynamic cultures with EA and CD microcarriers showed a significantly higher particle yield (5.5- and 6.0-fold, respectively) compared to the ST control, but did not differ from each other (Table 2). These findings are consistent with those of Haraszti et al., who observed a 20-fold increase in the exosome yield in a spinner flask using non-porous microcarriers compared to static cultures [11]. CD cultures were inoculated with a relatively high initial cell concentration of 53×10^3 cells mL^{-1} (ST: 19×10^3 cells mL^{-1}, EA: 22×10^3 cells mL^{-1}) to achieve the same inoculation cell density (cells cm^2) due to the large surface area of CD microcarriers. At the same time, the CD cultures reached a significantly lower final cell concentration of 28×10^4 cells mL^{-1} (ST: 112×10^4 cells mL^{-1}, EA: 56×10^4 cells mL^{-1}) due to a low expansion factor. Therefore, a very high initial cell number, rather than strong cell growth, could explain the similarly high particle yield compared to EA cultures.

The ST control as well as cultures with EA microcarriers had similar initial cell concentrations. Although the final cell concentration was twice as high in the ST control, the particle yield was lower. This indicated an increased particle production, especially on EA microcarriers. Another group suggested the calculation of a yield coefficient that is based on the total particle count, the initial cell count and the EV/particle production time for a better comparison [34]. Based on this yield coefficient, we reached 32×10^3 particles cell^{-1}·day^{-1} for ST, 30×10^3 particles cell^{-1}·day^{-1} for EA and 12×10^3 particles cell^{-1}·day^{-1} for CD cultures. In this case, the ST control and the non-porous EA microcarrier culture were more efficient in the EV production than CD cultures. Pinto et al. reached a yield coefficient of 36×10^3 particles cell^{-1}·day^{-1}, which is slightly higher than that we observed [34,35]. This might be due to a short-term high-shear EV production phase, used in their process. Since several studies mention shear stress, positively influencing and triggering MSC-EV production [8,11,13,36,37], we also expected and could finally confirm higher particle production rates in spinner flasks. The switching to a dynamic system triggers hMSC-TERT particle production rates independent of growth characteristics and microcarrier types due to hydrodynamic shear stress or shear stress induced by microcarrier collisions. This was also shown in other bioreactor types as Almeida Fuzeta et al. were able to increase the MSC-EV productivity by a factor of 3 and the particle production rate by a factor of 5, compared to static conditions when switching to an EA microcarrier-based culture in a vertical-wheel bioreactor [8].

We were aware that quantification of EVs using nanoparticle tracking analysis (NTA) has its limitations primarily stemming from the inability to decipher EVs from other particles of similar size such as protein precipitates, salt crystals and lipoprotein agglomerates. However, the lack of therapeutic potential of those particles without EV specificity has not yet been proven. We thus considered the totality of particles in the supernatant in the typical size range of MSC-EVs as MSC-derived particles including EVs and determined the therapeutic potency. However, for the quantification of explicit MSC-EVs, single-EV analytical techniques including imaging flow cytometry (IFCM), novel generations of flow cytometers or plasmon resonance devices with fluorescence detection units should be used. They allow the distinction between two different fluorescent labels including an EV-specific lipid dyes (i.e. Exoria) and MSC-EV specific epitope markers (i.e. CD81, CD63, CD9), while the EV nature of particles can be confirmed by the dissolution of particles after addition of detergents such as a NP-40 solution [38].

The size distribution profiles of all cultivations did not show any substantial differences as shown by a representative size distribution profile at the point in time of particle harvest for migration assay (Supplementary Figure 2). Therefore, we determined the overall mean particle size in supernatants over the whole cultivation process (Figure 1D). While larger particles (up to 5 μm) tend to be attributed to apoptotic bodies without relevant therapeutic potentials, exosomes and microvesicles are between 50 and 200 nm in size and have been proposed to be major mediators of therapeutic potencies [39]. We observed no differences in size between particles from ST, EA or SP cultures. Only following the transition from static to dynamic conditions had no impact on the particle size. However, the particles from cultures with both porous microcarrier types (CD and CP) showed a significantly smaller mean particle size of 133.4 ± 6 nm. Therefore, microcarrier porosity and, consequently, altered growth and particle production properties affected mean particle size. Compared to the size of EVs derived from hMSC-TERTs reported to be 90–150 nm in the literature [31,32], the detected particle sizes were within or slightly above this range.

3.1.3. EV surface epitope marker expression

To further characterize the particles and identify EVs, surface epitope markers were determined using the MACSPlex Exosome Kit in EA, CD, SP and ST supernatants. As we neither determined cell growth, nor an increase in particle production, we did not consider the CP samples for EV analysis. For normalization, the same particle count of 3.7×10^8 was analyzed in all set-ups. Since only particles above 100 nm were considered for the particle analysis used here, exosomes (<100 nm) could not be normalized in the surface epitope marker analysis. The observed altered mean fluorescence intensities (MFIs) could therefore also originate from non-quantified exosomes, which must be investigated in further experiments. We further focused on markers that are currently classified as EV specific markers, e.g., CD81, CD63 and CD9, or as MSC-specific markers, e.g., CD44 and CD29 [40]. Interestingly, the SP cultures, which had the highest particle production, showed no or only very low MFIs for all these markers (Figure 2A). We therefore concluded that these particles were not assigned EVs, so that we did not further investigate these samples. However, we must be aware that we carried out a normalization to a certain particle number for the EV marker analysis, regardless of the real EV number. If we consider that during the spheroid production process many particles in the same size range as EVs were formed due to surface-erosive processes, we can deduce that our samples likely had only few measurable EVs in them. To evaluate the real potential of the spheroid culture system, the EV fraction must be isolated and concentrated before analysis. With an EV isolation before analysis, other groups showed that MSCs as spheroids released increased amounts of potent EVs, compared to a 2D control [10,41,42].

The particles produced in ST, EA and CD cultures showed the presence of EV- and MSC-specific markers. CD81 and CD63, which belong to the group of tetraspanins, reached high MFIs in all set-ups (ST, CD and EA), confirming the release of EVs. In addition to CD63 and CD81, CD9 is also often mentioned as an EV-specific marker. However, this statement cannot be confirmed with the results of this work since, compared to CD63 and CD81, the CD9 expression was about 4 times lower. Interesting in this context are the results of Munshi et al., who also could not detect a CD9 expression on EVs derived from an immortalized (bm-MSC) cell line [43]. They found different levels of CD9 expression on EVs derived from five different bm-MSCs. These results indicate that a CD9 expression on EVs is dependent on cell types and cell origin and cannot necessarily be considered as an EV specific marker. We found that EA and CD culture samples had a significantly higher MFI of CD63 and CD44, compared to the ST control. Higher MFIs of CD63 could be an indicator for a larger EV fraction among the measured particles triggered by dynamic conditions, as discussed before. CD44 is an adhesion molecule and, together with CD29, known as a surface mediator for migration [44,45]. Both could enhance the homing of target cells to injured tissue sites and could show their therapeutic potency. The comparison of cultures with EA and CD microcarriers only showed a significant difference in CD29, which was increased by using micro-porous CD microcarriers. Since CD9 and CD29 MFIs are higher in CD cultures than in ST and EA cultures, we concluded that culture conditions and the microcarrier type not only affect particle production, but also surface epitope marker expression.
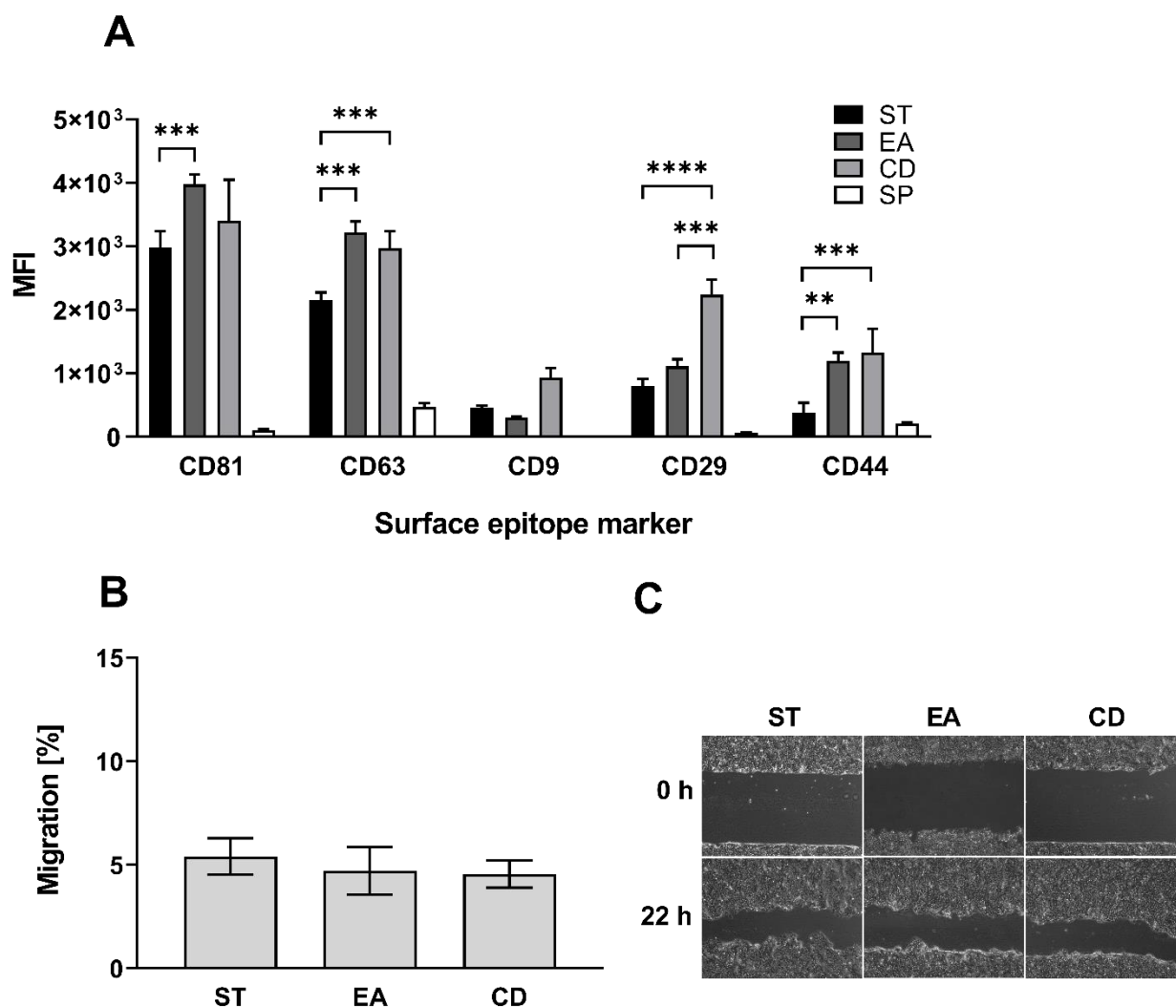
Figure 2. MSC-derived particle analysis produced in static (ST) and on different microcarriers in spinner flasks (Enhanced Attachment (EA), Cytodex 1 (CD)). (A) Background-subtracted mean fluorescence intensities (MFIs) (B) Potency of MSC-derived particles from different culture supernatants (ST, EA and CD) using a migration assay with HaCaT cells. (D) Representative images of gap after 0 h and 22 h. Data are presented as means ± SD (n = 3).

3.1.4. Potency assay

Probably the most important criterion for the evaluation of different MSC-derived particle production platforms is the therapeutic potency. We evaluated potency using a migration/scratch assay. For this, the migratory behavior of HaCaT cells was observed over 22 h after cell monolayer had been scratched by a pipette tip (Figure 2B, C). Our results were consistent with previous studies showing that applied MSC-derived particles including EVs improved cell proliferation and migration [46,47]. Interestingly, particles from ST control and dynamic culture conditions, regardless of the microcarrier type (EA and CD), promoted migration in the same manner. Hence, no direct correlation between

particle size or surface marker expression and therapeutic potency was observed. Since it is described in the literature that shear stress can modulate EV cargo resulting in an increase of EV potency [13,36], higher migration in dynamic EA and CD cultures was expected. Moreover, in different regeneration studies of different tissue types, EVs derived from cells cultured in 3D systems or treated with chemical or physical stimulation showed increased potency compared to EVs derived from 2D controls [34]. On the other hand, our results are consistent with those of Patel et al. who stated no significant gap closure difference of HDMECs treated with EVs from static flask, scaffold and bioreactor cultures [48]. Furthermore, the hypothesis that particles with increased CD29 and CD44 expression could lead to an increased potency was not confirmed. In addition to the surface epitope markers discussed in section 3.1.3, CD73 has been identified as a critical bioactive component in numerous studies. This molecule was investigated for its role in immunomodulatory effects, with evidence provided in the literature [49–51], as well as its involvement in wound healing processes [52]. Contrarily, another study has presented inconclusive results, revealing that CD73 activity did not correlate with performance in a multi-donor mixed lymphocyte reaction [53]. These findings indicate a complexity in the functional role of transmembrane enzymes such as CD73 that needs further investigation. The exploration of additional bioactive molecules may offer more comprehensive insights into the mode of action of MSC-derived particles including EVs. By rigorously defining their expression and activity, possible correlations with therapeutic potential may be established. This could lead to the identification of mediators that are possibly influenced by process transfers, thereby enhancing our understanding of the functional dynamics of MSC-derived particles including EVs. Moreover, it should be noted that for the migration assay, a corresponding control was created for each sample through ultrafiltration, which was then verified for the depletion of all particles using NTA. However, we have to admit that, although we created corresponding controls with identical microenvironments for each sample, there exists the possibility that the full therapeutic potential, perhaps even stronger, may have been masked by metabolic components. We recommend additional purification steps such as ultracentrifugation or tangential flow filtration (TFF) and rebuffering into standardized buffers to accurately assess the full therapeutic potentials of MSC-derived particles including EVs. It is important to note, however, that these purification methods may themselves affect EV preparations, which could again result in masking the true therapeutic potential [11].

The multifaceted and wide-ranging therapeutic efficacy of MSC-derived particles including EVs underscores their paramount significance in clinical applications. However, the diverse therapeutic potential is not a homogenous trait, rather, it stems from the distinct reactivity of various MSC types to external stimuli, which in turn shapes the production of MSC-derived particles and their properties, including therapeutic potential [2,6]. Thus, it is plausible that our alterations in culture conditions induced changes in the physicochemical characteristics of MSC-EVs, such as size and epitope markers, without effecting the potency of the particles on the migratory behavior of HaCaT cells. This underscores the pressing need for commercially available and standardized potency assays that can comprehensively evaluate the intricate therapeutic potential of MSC products [54]. There is no gold standard for EV analysis and due to heterogeneity of EVs, characterization by multiple, complementary techniques is important [21]. Different methods are currently being tested and regarding a standardized EV characterization the ISEV recommends the following method sequence: 1) quantitative measurement of the EV source (number of secreting cells) 2) total particle count 3) testing of components associated with EVs or EV-subtypes 4) testing for the presence of non-vesicular, co-isolated components [21]. Additionally, rather than surface epitope markers or EV size, the

composition of EV cargo, e.g., RNA and miRNA, should be investigated and determined in future, as these functional molecules are often considered to play a significant role in EV potencies. For instance, Haraszti et al. showed that MSC-EVs derived from an microcarrier-based system and isolated using tangential flow filtration were seven times more potent in delivery of small interfering RNA (siRNA) to neurons compared to MSC-EVs derived from a static system and isolated using ultracentrifugation [11]. We further recommend the cargo analysis using omics (genomics, proteomics, metabolomics, metagenomics, phenomics and transcriptomics) for the collective characterization and quantification of pools of biological molecules.

Our small-scale screening experiments demonstrated that MSCs were highly sensitive to culture conditions, even when MSC surface markers were not affected. However, the transition from static to dynamic conditions not only changed cellular growth characteristics (improvement on non-porous EA microcarriers), but also altered the production of MSC-derived particles. At the same time, only supernatants from proliferating cultures (EA, CD and ST) confirmed the presence of EVs and showed therapeutic potency in a migration/scratch assay. The particle load with EV- and MSC-specific markers were much higher in EA and CD cultures, although these particles were similar potent than those from ST controls. Therefore, the dynamic set-up is favorable as it gives more particles with a similar potency.

3.2. Evaluation of MSC-EV production in a 1 L STR

STRs offer several advantages over static and spinner flask cultures to produce MSCs or MSC-derived products such as EVs. The improved control of culture conditions, increased productivity, scalability, a homogeneous microenvironment and high reproducibility due to process analytical technology (PAT) make STRs a preferred choice for large-scale manufacturing [2]. Depending on our data, we transferred the process into a 1 L STR using EA microcarriers and investigated growth and particle key parameters in three independent STR runs (Figure 3). The cells in the STR grew with a comparable growth rate (0.032 ± 0.009 h^{-1}) to the ST control (0.031 ± 0.001 h^{-1}) but slightly lower than in spinner flasks. In parallel, the expansion factor decreased by 27% and 45% compared to ST control and EA microcarrier spinner cultures, respectively (Table 2 and Table 3).
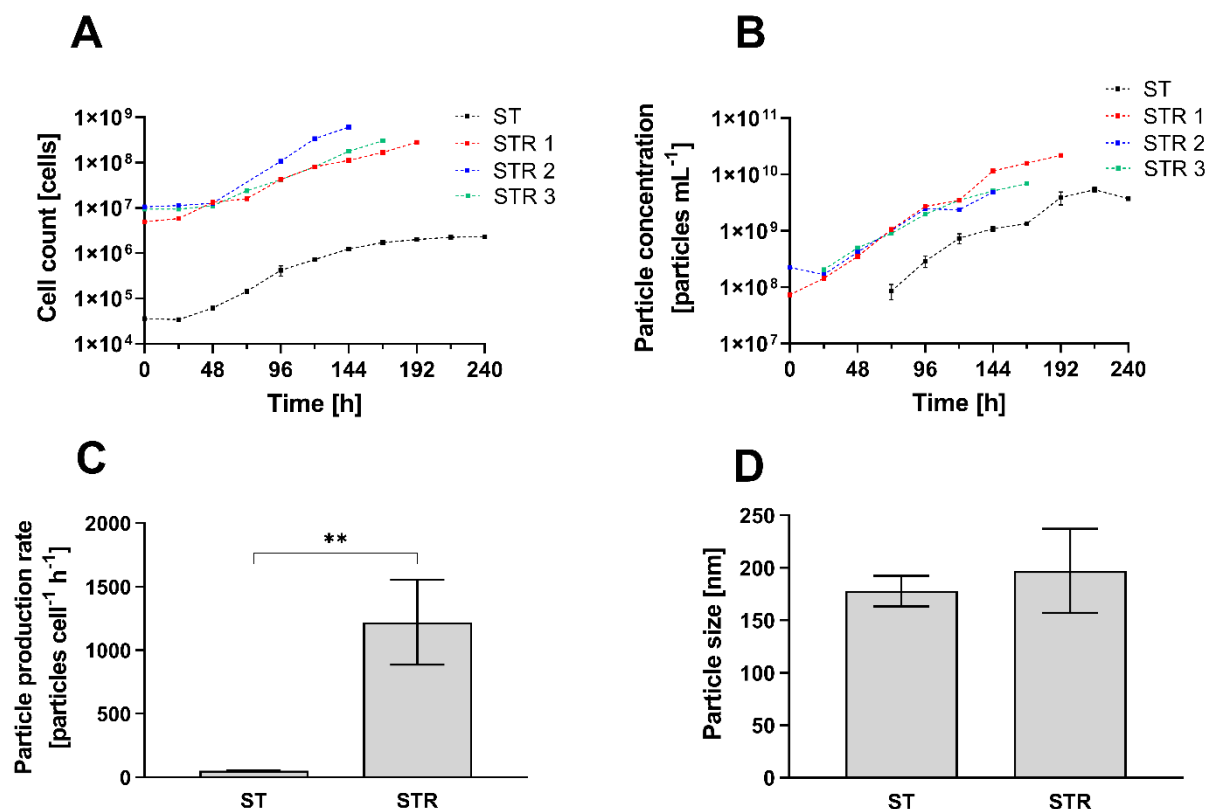
Figure 3. Analysis of MSC growth and particle production in static (ST) and dynamic cultures in three independent stirred tank bioreactors (STR) with EA microcarriers. (A) MSC count and (B) Particle concentration over time. (C) Particle production rate over the exponential growth phase (STR 1: 24–192 h, STR 2: 48–120 h, STR 3: 48–144 h). (D) Mean particle sizes. Data are presented as means ± SD (n = 3).

In the STRs, we determined a 3-fold increased particle concentration compared to the ST control (Figure 3B). Additionally, the particle production rate of 1219 ± 334 particles cell$^{-1} \cdot$h^{-1} during the exponential growth phase was 24.1 times higher compared to the ST control and 3.8 times higher compared to the spinner cultures (Figure 1C and Figure 3C). Thus, the process transfer from the spinner flask to a 1 L STR further stimulated particle production. Accordingly, a high particle yield was observed (27.5-fold to the ST control, 5-fold to the spinner cultures, Table 2 and Table 3), despite a similar initial cell concentration and a simultaneously lower final cell concentration of 45×10^4 cells mL^{-1} (ST: 112×10^4 cells mL^{-11}). We also calculated the alternative yield coefficient, which refers to the total number of EV/particles, the initial cell count and production time [34]. Here, this yield coefficient was significantly increased to 66×10^3 particles cell$^{-1} \cdot$day^{-1} (ST: 32×10^3 particles cell$^{-1} \cdot$day^{-1}, Spinner: 30×10^3 particles cell$^{-1} \cdot$day^{-1}). The mean size of the particles was not affected (197 ± 40 nm) by the transfer into the STRs (Figure 3D). The underlying mechanisms for an increased particle production in the STRs are not yet fully understood. One explanation might be the differences in the hydrodynamic flow regime. Whereas a turbulent medium flow profile is present in the STR, spinner flasks often form a rather laminar flow. Therefore, also the shear forces acting on the MSCs on microcarriers in the spinner flask are lower, compared to the STR. Since it is already known that

the MSC-EV production responds to external stimuli such as shear stress, this may confirm that higher shear stress levels will also result in an increased particle production. In fact, in the literature it is reported that by increasing the stirrer speed in a spinner culture, thus generating more turbulence and more shear stress, the EV production per cell was increased [34]. Another major difference between the ST control/spinner flask and the STR is that process parameters, such as pH and dissolved oxygen (DO) levels, are fully controlled and kept constant in the STR. Accordingly, besides the changed fluid flow profile in the STR, constant levels of pH and DO could favor the production of MSC-EVs. This highlights the need for a better process knowledge and the determination of critical process parameters for MSC-EV production processes.

The metabolic conversion rates in the STRs (Table 3), e.g., the glucose consumption and lactate formation rates, did not differ significantly from those of the spinner flask system (Table 2). However, the linear correlation between the particle production rate and the glucose consumption rate, which were previously determined in spinner flask cultures, was not confirmed for the STRs. This correlation underestimated the actual particle production rate by a factor of 4 and was therefore not applicable. Therefore, further investigations are necessary to develop a deeper understanding and define limitations to identify possible correlations for further MSC-EV process development. To elaborate on the operational efficiency of the STR process, a yield coefficient of produced particles per unit glucose can be used. In comparison to the ST control, which yielded approximately 7×10^{11} particles per gram of glucose, the STR process exhibited a significant increase in the yield coefficient, amounting to a 7-fold rise, resulting in 50×10^{11} particles per gram of glucose.

Table 3. Overview of relevant biological properties of MSCs and produced particles in static and stirred tank bioreactor (STR) cultures, such as growth rate, expansion factor, particle yield and specific metabolic key parameters as the glucose consumption and lactate production rate. Data are presented as means ± SD (n = 3).

System	Growth rate [h^{-1}]	Expansion factor [-]	Particle yield [10^3 Particles cell^{-1}]	Glucose consumption rate [10^{-12} g·cell^{-1}·h^{-1}]	Lactate production rate [10^{-12} g·cell^{-1}·h^{-1}]
ST	0.031 ± 0.001	67.4 ± 8.5	1.6 ± 0.1	70 ± 5	81 ± 5
STR	0.032 ± 0.009	49.0 ± 11.8	45 ± 22	241 ± 104	185 ± 28

The EV surface epitope markers of MSC-derived particles in supernatants in the STR were analyzed using the MACSPlex exosome kit (Figure 4A). Significant differences were observed between the ST control and the STRs, while all EV- and MSC-specific markers were highly expressed in the supernatants of the STR. The EV-typical surface epitope markers (CD81 and CD63) were significantly higher, indicating a larger EV fraction in the STR than in the ST control. In addition, these MFIs of the samples from the STR cultures were higher, compared to the MFIs detected in spinner flasks with EA microcarriers (Figure 2A).

The therapeutic potency was again evaluated, using a migration assay with HaCaT cells (Figure 4B,C). Similar to the spinner flask culture, no significant difference (p = 0.13) in the migratory behavior of HaCaT cells, triggered by MSC-derived particles including EVs from STRs, was detected. However, a trend emerged that an increased expression of EV- and MSC-specific markers is also associated with an increased therapeutic potency.
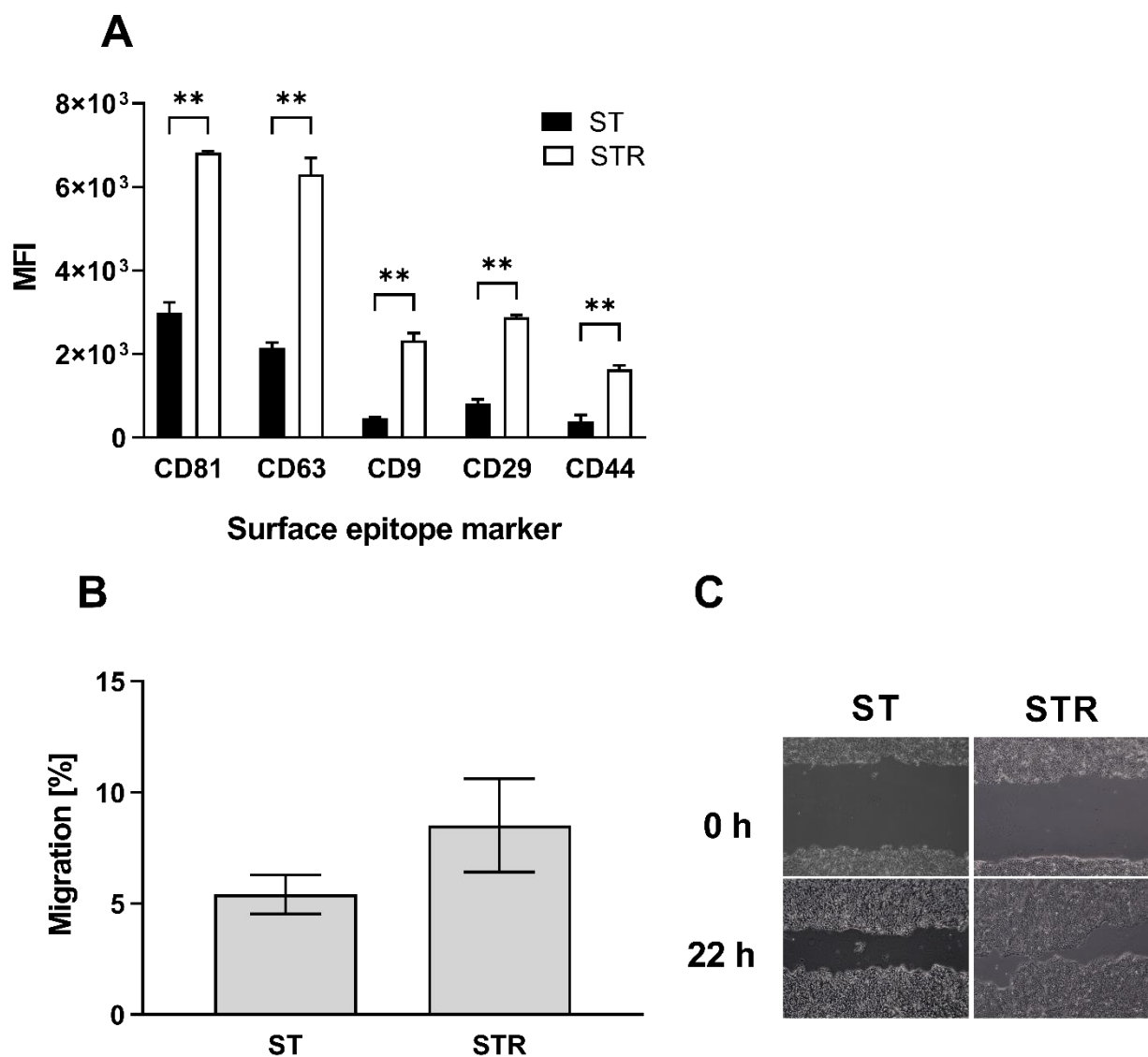
Figure 4. MSC-derived particle analysis produced in static and STR cultures. (A) Background-subtracted mean fluorescence intensities (MFIs). (B) Potency of MSC-derived particles using a migration with HaCaT cells (p = 0.13). (C) Representative images of gap after 0 h and 22 h. Data are presented as means ± SD (n = 3).

In total, the STRs yielded 10^{13} particles, which outperformed classical, static cultures. To be precise, for a comparable number of particles as in a 1 L STR, including its EV release-promoting effects, 200 T-75 or over 85 T-175 flasks would be required to maintain the surface to volume ratio

of 5.4 cm^2·mL^{-1}, entailing higher costs for materials and operators and showing the limitations of scaling out standard cell culture vessels. Thus, we have demonstrated that fully controlled stirred-tank bioreactors, using non-porous microcarriers, represent a potent production platform for MSC-derived particles including EVs, enabling a rigorous process control and thereby laying the groundwork for clinical applications.

4. Conclusions

In this study, we have demonstrated that the production of MSC-derived particles including EVs can be effectively increased in dynamic systems, such as spinner flasks or STR. Our results highlight the critical role of culture conditions on both cell growth and EV production. Specifically, we found that non-porous microcarriers exhibited superior cell growth and particle production compared to porous microcarriers. Conversely, the use of MSC spheroids as a culture strategy was not ideal for EV production. Although MSC spheroids outperformed all other systems in the number of EV-sized particles, most of these particles showed no EV- or MSC-specific markers. Interestingly, we observed that increased particle production rates in dynamic systems were not directly linked to enhanced growth properties, but to an enhanced cellular metabolism (glucose consumption). Although we did observe some differences in the EV epitope markers between static and dynamic culture methods, all platforms demonstrated comparable a therapeutic potency in a migration assay. We could successfully transfer the EV production process into a fully controlled 1 L STR using non-porous microcarriers. Notably, the growth characteristics of the cells remained unchanged, but the particle production rate substantially increased. Additionally, there was a trend towards an increased therapeutic potency. The absolute yield of MSC-derived particles including EVs from one 1 L STR was equivalent to that of over 200 T75 flasks, underscoring the scalability and reproducibility of our STR-based production process. In summary, our study provides valuable insights into relevant process parameters and the optimization of an MSC-derived particle production and highlights the potential of a scalable, monitored and controlled EV manufacturing in STRs.

Use of AI tools declaration

The authors declare they have not used Artificial Intelligence (AI) tools in the creation of this article.

Acknowledgments

Conflict of interest

The authors declare no conflict of interest.

Author Contributions:

J.B. conceived, designed the experiments, and wrote the paper. J.F. wrote parts of the first draft. M.O. and L.R. assisted with the experiments. D.E. helped to draft. D.S. and P.C. revised the manuscript, supervised the research, and acquired funding. All authors have read and agreed to the published version of the manuscript.

References

1. Egger D, Tripisciano C, Weber V, et al. (2018) Dynamic cultivation of mesenchymal stem cell aggregates. *Bioengineering* 5: 48. https://doi.org/10.3390/bioengineering5020048

2. Barekzai J, Petry F, Czermak P, et al. (2022) Process design for human mesenchymal stem cell products in Stirred-Tank bioreactors, In: Pörtner, R., *Cell Culture Engineering and Technology: In appreciation to Professor Mohamed Al-Rubeai,* Cham: Springer International Publishing, 307–333. https://doi.org/10.1007/978-3-030-79871-0_10

3. Barekzai J, Petry F, Zitzmann J, et al. (2020) Bioprocess development for human mesenchymal stem cell therapy products, In: María Martínez-Espinosa, R., *New Advances on Fermentation Processes,* United kingdom: IntechOpen, 1–25. https://doi.org/10.5772/intechopen.90029

4. Phan J, Kumar P, Hao D, et al. (2018) Engineering mesenchymal stem cells to improve their exosome efficacy and yield for cell-free therapy. *J Extracell Vesicles* 7: 1522236. https://doi.org/10.1080/20013078.2018.1522236

5. Varderidou-Minasian S, Lorenowicz MJ (2020) Mesenchymal stromal/stem cell-derived extracellular vesicles in tissue repair: challenges and opportunities. *Theranostics* 10: 5979–5997. https://doi.org/10.7150/thno.40122

6. Almeria C, Kreß S, Weber V, et al. (2022) Heterogeneity of mesenchymal stem cell-derived extracellular vesicles is highly impacted by the tissue/cell source and culture conditions. *Cell Biosci* 12: 51. https://doi.org/10.1186/s13578-022-00786-7

7. Ng CY, Kee LT, Al-Masawa ME, et al. (2022) Scalable production of extracellular vesicles and its therapeutic values: a review. *Int J Mol Sci* 23: 7986. https://doi.org/10.3390/ijms23147986

8. Almeida Fuzeta Mde, Bernardes N, Oliveira FD, et al. (2020) Scalable production of human mesenchymal stromal cell-derived extracellular vesicles under serum-/xeno-free conditions in a microcarrier-based bioreactor culture system. *Front Cell Dev Biol* 8: 553444. https://doi.org/10.3389/fcell.2020.553444

9. Cao J, Wang B, Tang T, et al. (2020) Three-dimensional culture of MSCs produces exosomes with improved yield and enhanced therapeutic efficacy for cisplatin-induced acute kidney injury. *Stem Cell Res Ther* 11: 206. https://doi.org/10.1186/s13287-020-01719-2

10. Cha JM, Shin EK, Sung JH, et al. (2018) Efficient scalable production of therapeutic microvesicles derived from human mesenchymal stem cells. *Sci Rep* 8: 1171. https://doi.org/10.1038/s41598-018-19211-6

11. Haraszti RA, Miller R, Stoppato M, et al. (2018) Exosomes produced from 3D cultures of MSCs by tangential flow filtration show higher yield and improved activity. *Mol Ther* 26: 2838–2847. https://doi.org/10.1016/j.ymthe.2018.09.015

12. Fernandes-Platzgummer A, Cunha R, Morini S, et al. (2023) Optimized operation of a controlled stirred tank reactor system for the production of mesenchymal stromal cells and their extracellular vesicles. *Biotechnol Bioeng* 120: 2742–2755. https://doi.org/10.1002/bit.28449

13. Piffoux M, Nicolás-Boluda A, Mulens-Arias V, et al. (2019) Extracellular vesicles for personalized medicine: The input of physically triggered production, loading and theranostic properties. *Adv Drug Deliver Rev* 138: 247–258. https://doi.org/10.1016/j.addr.2018.12.009

14. Staubach S, Bauer FN, Tertel T, et al. (2021) Scaled preparation of extracellular vesicles from conditioned media. *Adv Drug Deliver Rev* 177: 113940. https://doi.org/10.1016/j.addr.2021.113940

15. Kornilov R, Puhka M, Mannerström B, et al. (2018) Efficient ultrafiltration-based protocol to deplete extracellular vesicles from fetal bovine serum. *J Extracell Vesicles* 7: 1422674. https://doi.org/10.1080/20013078.2017.1422674

16. Adlerz K, Patel D, Rowley J, et al. (2020) Strategies for scalable manufacturing and translation of MSC-derived extracellular vesicles. *Stem Cell Res* 48: 101978. https://doi.org/10.1016/j.scr.2020.101978

17. Leber J, Barekzai J, Blumenstock M, et al. (2017) Microcarrier choice and bead-to-bead transfer for human mesenchymal stem cells in serum-containing and chemically defined media. *Process Biochem* 59: 255–265. https://doi.org/10.1016/j.procbio.2017.03.017

18. Lawson T, Kehoe DE, Schnitzler AC, et al. (2017) Process development for expansion of human mesenchymal stromal cells in a 50L single-use stirred tank bioreactor. *Biochem Eng J* 120: 49–62. https://doi.org/10.1016/j.bej.2016.11.020

19. Lembong J, Kirian R, Takacs JD, et al. (2020) Bioreactor parameters for microcarrier-based human MSC expansion under xeno-free conditions in a vertical-wheel system. *Bioengineering* 7: 73. https://doi.org/10.3390/bioengineering7030073

20. Mizukami A, Fernandes-Platzgummer A, Carmelo JG, et al. (2016) Stirred tank bioreactor culture combined with serum-/xenogeneic-free culture medium enables an efficient expansion of umbilical cord-derived mesenchymal stem/stromal cells. *Biotechnol J* 11: 1048–1059. https://doi.org/10.1002/biot.201500532

21. Théry C, Witwer KW, Aikawa E, et al. (2018) Minimal information for studies of extracellular vesicles 2018 (MISEV2018): a position statement of the international society for extracellular vesicles and update of the MISEV2014 guidelines. *J Extracell Vesicles* 7: 1535750. https://doi.org/10.1080/20013078.2018.1535750

22. Simonsen JL, Rosada C, Serakinci N, et al. (2002) Telomerase expression extends the proliferative life-span and maintains the osteogenic potential of human bone marrow stromal cells. *Nat Biotechnol* 20: 592–596. https://doi.org/10.1038/nbt0602-592

23. Petry F, Salzig D (2022) Large-scale production of size-adjusted β-Cell spheroids in a fully controlled stirred-tank reactor. *Processes* 10: 861. https://doi.org/10.3390/pr10050861

24. Zwietering T (1958) Suspending of solid particles in liquid by agitators. *Chem Eng Sci* 8: 244–253. https://doi.org/10.1016/0009-2509(58)85031-9

25. Peter CP (2007) Design of shaken bioreactors for fermentation systems with elevated viscosity and hydromechanical sensibility [PhD thesis], Aachen: Publication server of RWTH Aachen University.

26. Jaccard N (2015) Development of an image processing method for automated, non-invasive and scale-independent monitoring of adherent cell cultures [PhD thesis], London: University College London.

27. Yang Y, Rossi FMV, Putnins EE (2007) Ex vivo expansion of rat bone marrow mesenchymal stromal cells on microcarrier beads in spin culture. *Biomaterials* 28: 3110–3120. https://doi.org/10.1016/j.biomaterials.2007.03.015

28. Salzig D, Leber J, Merkewitz K, et al. (2016) Attachment, growth, and detachment of human mesenchymal stem cells in a chemically defined medium. *Stem Cells Int* 2016: 5246584. https://doi.org/10.1155/2016/5246584

29. Elseberg CL, Leber J, Salzig D, et al. (2012) Microcarrier-based expansion process for hMSCs with high vitality and undifferentiated characteristics. *Int J Artif Organs* 35: 93–107. https://doi.org/10.5301/ijao.5000077

30. Petry F, Salzig D (2022) The cultivation conditions affect the aggregation and functionality of β-cell lines alone and in coculture with mesenchymal stromal/stem cells. *Eng Life Sci* 22: 769–783. https://doi.org/10.1002/elsc.202100168

31. Franquesa M, Hoogduijn MJ, Ripoll E, et al. (2014) Update on controls for isolation and quantification methodology of extracellular vesicles derived from adipose tissue mesenchymal stem cells. *Front Immunol* 5: 525. https://doi.org/10.3389/fimmu.2014.00525

32. L Ramos T, Sánchez-Abarca LI, Muntión S, et al. (2016) MSC surface markers (CD44, CD73, and CD90) can identify human MSC-derived extracellular vesicles by conventional flow cytometry. *Cell Commun Signaling* 14: 2. https://doi.org/10.1186/s12964-015-0124-8

33. Wang J, Bonacquisti EE, Brown AD, et al. (2020) Boosting the biogenesis and secretion of mesenchymal stem cell-derived exosomes. *Cells* 9: 660. https://doi.org/10.3390/cells9030660

34. Grangier A, Branchu J, Volatron J, et al. (2021) Technological advances towards extracellular vesicles mass production. *Adv Drug Delivery Rev* 176: 113843. https://doi.org/10.1016/j.addr.2021.113843

35. PPinto A, Marangon I, Méreaux J, et al. (2021) Immune reprogramming precision photodynamic therapy of peritoneal metastasis by scalable stem-cell-derived extracellular vesicles. *ACS Nano* 15: 3251–3263. https://doi.org/10.1021/acsnano.0c09938

36. Patel DB, Santoro M, Born LJ, et al. (2018) Towards rationally designed biomanufacturing of therapeutic extracellular vesicles: impact of the bioproduction microenvironment. *Biotechnol Adv* 36: 2051–2059. https://doi.org/10.1016/j.biotechadv.2018.09.001

37. Grangier A, Wilhelm C, Gazeau F, et al. (2020) High yield and scalable EV production from suspension cells triggered by turbulence in a bioreactor. *Cytotherapy* 22: 50. https://doi.org/10.1016/j.jcyt.2020.03.061

38. Tertel T, Schoppet M, Stambouli O, et al. (2022) Imaging flow cytometry challenges the usefulness of classically used extracellular vesicle labeling dyes and qualifies the novel dye Exoria for the labeling of mesenchymal stromal cell-extracellular vesicle preparations. *Cytotherapy* 24: 619–628. https://doi.org/10.1016/j.jcyt.2022.02.003

39. Murphy DE, de Jong OG, Brouwer M, et al. (2019) Extracellular vesicle-based therapeutics: natural versus engineered targeting and trafficking. *Exp Mol Med* 51: 1–12. https://doi.org/10.1038/s12276-019-0223-5

40. Skovronova R, Grange C, Dimuccio V, et al. (2021) Surface marker expression in small and medium/large mesenchymal stromal cell-derived extracellular vesicles in naive or apoptotic condition using orthogonal techniques. *Cells* 10: 2948. https://doi.org/10.3390/cells10112948

41. Yuan X, Sun L, Jeske R, et al. (2022) Engineering extracellular vesicles by three-dimensional dynamic culture of human mesenchymal stem cells. *J Extracell Vesicles* 11: e12235. https://doi.org/10.1002/jev2.12235

42. Zhang Y, Chopp M, Zhang ZG, et al. (2017) Systemic administration of cell-free exosomes generated by human bone marrow derived mesenchymal stem cells cultured under 2D and 3D conditions improves functional recovery in rats after traumatic brain injury. *Neurochem Int* 111: 69–81. https://doi.org/10.1016/j.neuint.2016.08.003

43. Munshi A, Mehic J, Creskey M, et al. (2019) A comprehensive proteomics profiling identifies NRP1 as a novel identity marker of human bone marrow mesenchymal stromal cell-derived small extracellular vesicles. *Stem Cell Res Ther* 10: 401. https://doi.org/10.1186/s13287-019-1516-2

44. Sierra-Parraga JM, Merino A, Eijken M, et al. (2020) Reparative effect of mesenchymal stromal cells on endothelial cells after hypoxic and inflammatory injury. *Stem Cell Res Ther* 11: 352. https://doi.org/10.1186/s13287-020-01869-3

45. Priglinger E, Strasser J, Buchroithner B, et al. (2021) Comprehensive label-free characterization of extracellular vesicles and their surface proteins. *J Extracell Vesicles*: e12156. https://doi.org/10.1002/jev2.12156

46. Cabral J, Ryan AE, Griffin MD, et al. (2018) Extracellular vesicles as modulators of wound healing. *Adv Drug Delivery Rev* 129: 394–406. https://doi.org/10.1016/j.addr.2018.01.018

47. Zhang J, Guan J, Niu X, et al. (2015) Exosomes released from human induced pluripotent stem cells-derived MSCs facilitate cutaneous wound healing by promoting collagen synthesis and angiogenesis. *J Transl Med* 13: 49. https://doi.org/10.1186/s12967-015-0417-0

48. Patel DB, Luthers CR, Lerman MJ, et al. (2019) Enhanced extracellular vesicle production and ethanol-mediated vascularization bioactivity via a 3D-printed scaffold-perfusion bioreactor system. *Acta Biomater* 95: 236–244. https://doi.org/10.1016/j.actbio.2018.11.024

49. Amarnath S, Foley JE, Farthing DE, et al. (2015) Bone marrow-derived mesenchymal stromal cells harness purinergenic signaling to tolerize human Th1 cells in vivo. *Stem Cells* 33: 1200–1212. https://doi.org/10.1002/stem.1934

50. Teo KYW, Zhang S, Loh JT, et al. (2023) Mesenchymal stromal cell exosomes mediate M2-like macrophage polarization through CD73/Ecto-5'-nucleotidase activity. *Pharmaceutics* 15: 1489. https://doi.org/10.3390/pharmaceutics15051489

51. Turiello R, Capone M, Morretta E, et al. (2022) Exosomal CD73 from serum of patients with melanoma suppresses lymphocyte functions and is associated with therapy resistance to anti-PD-1 agents. *J Immunother Cancer* 10: e004043. https://doi.org/10.1136/jitc-2021-004043

52. Hettich BF, Ben-Yehuda Greenwald M, Werner S, et al. (2020) Exosomes for wound healing: purification optimization and identification of bioactive components. *Adv Sci* 7: 2002596. https://doi.org/10.1002/advs.202002596

53. Bauer FN, Tertel T, Stambouli O, et al. (2023) CD73 activity of mesenchymal stromal cell-derived extracellular vesicle preparations is detergent-resistant and does not correlate with immunomodulatory capabilities. *Cytotherapy* 25: 138–147. https://doi.org/10.1016/j.jcyt.2022.09.006

54. Nguyen VVT, Witwer KW, Verhaar MC, et al. (2020): Functional assays to assess the therapeutic potential of extracellular vesicles. *J Extracell Vesicles* 10: e12033. https://doi.org/10.1002/jev2.12033